

Mapping of a New Deformation Region around ^{62}Ti

S. Michimasa^{1,*}, M. Kobayashi¹, Y. Kiyokawa¹, S. Ota¹, R. Yokoyama², D. Nishimura^{1,3}, D. S. Ahn^{4,†}, H. Baba⁴, G. P. A. Berg⁵, M. Dozono¹, N. Fukuda⁴, T. Furuno^{6,‡}, E. Ideguchi⁷, N. Inabe⁴, T. Kawabata^{6,§}, S. Kawase⁸, K. Kisamori¹, K. Kobayashi⁹, T. Kubo^{10,11,||}, Y. Kubota^{4,¶}, C. S. Lee^{1,**}, M. Matsushita¹, H. Miya¹, A. Mizukami¹², H. Nagakura⁹, H. Oikawa¹², H. Sakai⁴, Y. Shimizu⁴, A. Stolz¹¹, H. Suzuki⁴, M. Takaki¹, H. Takeda⁴, S. Takeuchi¹³, H. Tokieda¹, T. Uesaka⁴, K. Yako¹, Y. Yamaguchi¹, Y. Yanagisawa⁴, K. Yoshida⁴ and S. Shimoura¹

¹Center for Nuclear Study, The University of Tokyo, 2-1 Hirosawa, Wako, Saitama 351-0198, Japan

²Department of Physics and Astronomy, the University of Tennessee, Knoxville, Tennessee 37996, USA

³Department of Natural Sciences, Tokyo City University, Tamazutsumi 1-28-1, Setagaya-ku, Tokyo 158-8557, Japan

⁴RIKEN Nishina Center for Accelerator-Based Science, 2-1 Hirosawa, Wako, Saitama 351-0198, Japan

⁵Department of Physics and Joint Institute for Nuclear Astrophysics, University of Notre Dame, Notre Dame, Indiana 46556, USA

⁶Department of Physics, Kyoto University, Kitashirakawa-Oiwake, Sakyo, Kyoto 606-8502, Japan

⁷Research Center for Nuclear Physics, Osaka University, 10-1 Mihogaoka, Ibaraki, Osaka 567-0047, Japan

⁸Department of Advanced Energy Engineering Science, Kyushu University, 6-1 Kasuga-koen, Kasuga, Fukuoka 816-8580, Japan


⁹Department of Physics, Rikkyo University, Toshima, Tokyo 171-8501, Japan

¹⁰Facility for Rare Isotope Beams, Michigan State University, 640 S Shaw Lane, East Lansing, Michigan 48824, USA

¹¹National Superconducting Cyclotron Laboratory, Michigan State University, 640 S Shaw Lane, East Lansing, Michigan 48824, USA

¹²Department of Physics, Tokyo University of Science, Noda, Chiba 278-8510, Japan

¹³Department of Physics, Tokyo Institute of Technology, Meguro, Tokyo 152-8551, Japan

 (Received 3 April 2020; revised 12 June 2020; accepted 21 July 2020; published 14 September 2020)

We performed the first direct mass measurements of neutron-rich scandium, titanium, and vanadium isotopes around the neutron number 40 at the RIKEN RI Beam Factory using the time-of-flight magnetic-rigidity technique. The atomic mass excesses of $^{58-60}\text{Sc}$, $^{60-62}\text{Ti}$, and $^{62-64}\text{V}$ were measured for the first time. The experimental results show that the two-neutron separation energies in the vicinity of ^{62}Ti increase compared to neighboring nuclei. This shows that the masses of Ti isotopes near $N = 40$ are affected by the Jahn-Teller effect. Therefore, a development of Jahn-Teller stabilization appears below the Cr isotopes, and the systematics in Sc, Ti, and V isotopes suggest that ^{62}Ti is located close to the peak of the Jahn-Teller effect.

DOI: [10.1103/PhysRevLett.125.122501](https://doi.org/10.1103/PhysRevLett.125.122501)

The atomic nucleus is a self-consistent quantum system dominated by the nuclear interactions among protons and neutrons. The character of the interactions directly influences a mean-field shape and internal shell structures of individual nucleus. On the Fermi surface of a nucleus, the energy spacing of occupied and unoccupied orbitals is an indication of the robustness of the nucleus [1,2]. A degeneracy of these orbitals drives an onset of nuclear deformation through the Jahn-Teller (JT) effect [3,4], which is well known as a symmetry-breaking mechanism in various self-consistent quantum systems such as nonlinear molecules and crystals [5]. The main function of the JT effect is to obtain effectively the stability of the system by modifying its degeneracy. It is noteworthy that the JT effect provides a consistent explanation of the onset of deformations in the nuclei accompanying a magicity-loss phenomenon at $N = 8, 20$, and 28 [6]. Theoretical considerations suggest that this phenomenon is caused by the JT effect combined with shrinking of conventional energy gaps of single-particle levels in stable nuclei. Such a scenario is

supported by the experimental results of shell quenching and nuclear deformation in nuclei around $^{12}\text{Be}_8$ [7–9], $^{31}\text{Na}_{20}$ [10–12], and $^{44}\text{S}_{28}$ [13–16].

The structural change along the $N = 40$ isotones is a significant milestone to explain the close relation between shell evolution and stability in neutron-rich nuclei [17]. The deformation mechanism in neutron-rich nuclei around $N = 40$ is then considered to be similar to that in the so-called island-of-inversion nuclei around $N = 20$. The island of inversion expresses nuclear regions of deformation promoted by shell breaking associated with the magic numbers [18]. It is suggested that the nuclear central force and tensor interaction play key roles in the change of the single-particle levels in both nuclear regions [19–21]. As the number of protons is reduced in $\pi 1f_{7/2}$ ($\pi 1d_{5/2}$) in neutron-rich $N = 40$ (20) isotones, the tensor interactions weaken the binding of the spin-orbit part of the $\nu 1f_{5/2}$ ($\nu 1d_{3/2}$) orbital and simultaneously promote an intruder effect of the $\nu 1g_{9/2}$ ($\nu 1f_{7/2}$) and higher orbitals [22,23]. In order to survey a new region of deformation,

many experiments for Cr-Fe isotopes at $N \sim 40$ were performed to measure low-lying excitation energies [24–27], quadrupole collectivities [28,29], and atomic masses [30–32]. Those experimental results consistently support the onset of enhanced deformation at $Z = 24$ – 26 due to intruder effects of the upper $\nu g_{9/2}$ and $\nu d_{5/2}$ orbitals.

Recently the two experimental articles were published concerning the nuclear properties around ^{62}Ti . In ^{61}Ti , a candidate of an isomeric state at 700 keV in the $\nu g_{9/2}$ orbital was found [33]. This result indicates that a degeneracy between the fp and $g_{9/2}$ orbitals is indicated in Ti isotopes close to $N = 40$. Furthermore, it was reported that the 2_1^+ and 4_1^+ excitation energies in ^{62}Ti are located at 683(10) and 1506(22) keV [34]. The authors suggest that the configuration mixing between neutron fp and gd orbitals is significant in ^{62}Ti and that it tends to decrease from ^{64}Cr to ^{62}Ti .

In this Letter, we present the first mass measurements of the scandium, titanium, and vanadium isotopes far from stability, towards $N = 40$. This provides critical data to map the new island of inversion around $N = 40$. The measurement was performed by the time-of-flight magnetic-rigidity (TOF- $B\rho$) method [35,36] using the 105-meter beam line of the BigRIPS separator [37], the High-resolution beam line, and the SHARAQ spectrometer [38] at the RI Beam Factory (RIBF) at RIKEN. The experimental setup and analysis are described in detail in Ref. [39] and briefly summarized here. A schematic layout of the beam line with the locations of the detectors used in the experiment is shown in Fig. 1. The isotopes of interest were produced by fragmentation of a ^{70}Zn primary beam at 345 MeV/nucleon in a ^9Be target of 2.2 g/cm² thickness, purified by using a wedge degrader with the central thickness of 0.27 g/cm² at BigRIPS focus F1, and transported in the dispersion matched mode [40] to the final focal plane, S2. The momentum acceptance in this mode is $\pm 0.3\%$. A set of CVD diamond detectors [41] at F3 and S2 measured the TOF. The typical TOF was 540 ns. Low-pressure multiwire drift chambers (LP-MWDCs) [42] and a

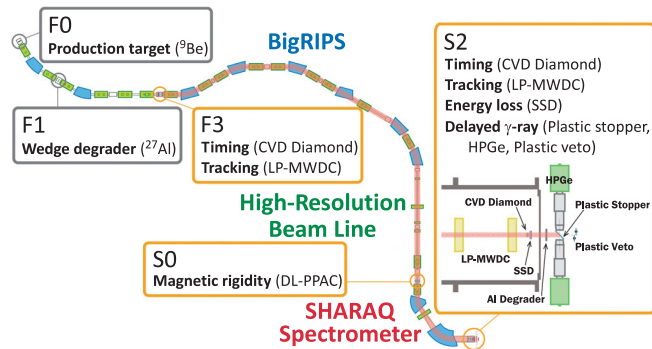


FIG. 1. Schematic layout of the BigRIPS separator, the High-resolution beam line, and the SHARAQ spectrometer. Detectors and equipment in the focal planes F0-F3, S0, and S2 are shown.

delay-line parallel-plate avalanche counter (DL-PPAC) [43] were used for beam tracking at the foci indicated in Fig. 1. Silicon strip detectors at S2 were installed for identification of the atomic number of the fragments. For isomer search of the isotopes, a detector system [44] consisting of a plastic stopper, two HPGc clover detectors [45] and a plastic veto detector was installed downstream of S2 to estimate the flux of isomer states in fragmented nuclei.

The mass of a fragment m is determined from the simultaneous measurement of the charge q , TOF t , magnetic rigidity $B\rho$, and flight path length L between the timing detectors by using the equation

$$\frac{m}{q} = \frac{B\rho}{\gamma L} t = \frac{B\rho}{c} \sqrt{\left(\frac{ct}{L}\right)^2 - 1}, \quad (1)$$

where γ is the Lorentz factor and c the speed of light. The required high accuracy of the mass is achieved with accurate ion-optical parameters for L and $B\rho$ determined by using tracking data. In practice, the atomic masses are determined by considering a fourth-order polynomial function of the ion-optical matrix elements, which were determined by a multiple polynomial regression of the ion-optical data of reference masses measured simultaneously.

Figure 2 shows the measured m/q spectrum of the scandium, titanium, and vanadium isotopes, where the masses of underlined nuclei are newly measured in the present experiment. The horizontal axis was calibrated by the reference masses measured simultaneously of $^{52-54}\text{Ca}$, $^{49,51-53}\text{K}$, $^{46-48}\text{Ar}$, $^{43-46}\text{Cl}$, $^{41,42}\text{S}$, $^{38-42}\text{P}$, and $^{36-40}\text{Si}$ [46–49]. The typical root-mean-square (rms) resolution of m/q for these isotopes is 1×10^{-4} . The reference masses are distributed in m/q in the range of 2.527–2.857 amu/e and thus cover all the isotopes of interest. The m/q values of the reference masses were systematically reproduced within an error of 6.1 keV/e, which is perceived to be the systematic error in this

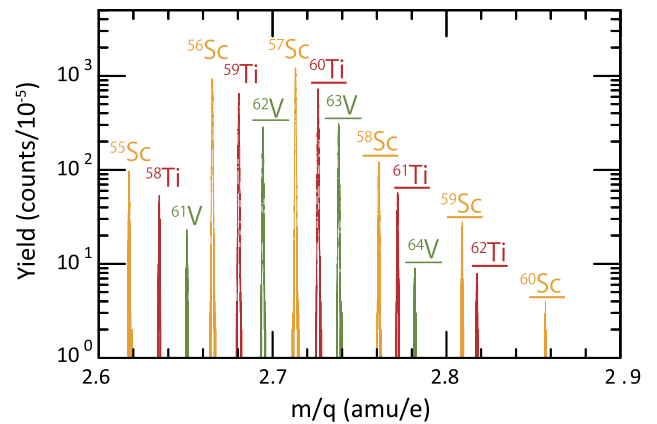


FIG. 2. Measured m/q spectrum of Sc, Ti, and V isotopes. The masses of underlined isotopes are newly determined in the present experiment.

TABLE I. The isomeric γ decays identified in the present experiment and previously reported values.

Nucleus	E_γ (keV)	$T_{1/2}$ (μ s)	I_γ (%)	Ref.
^{61}Ti	125.2(6), 576.1(5)	0.3(1), 0.2(1)	62(33), 100(51)	Present
	125.0(5), 575.1(5)	0.200(28), 0.354(69)	...	[33]
^{59}Ti	108.9(4)	0.61(2)	100	Present
	108.5(5)	0.618(12)	100	[33]
^{58}Sc	180.5(6), 247(2), 412.3(6), 580.9(4)	0.6(2), 1.3(8), 0.9(5), 0.5(2)	27(14), 26(19), 85(36), 100(43)	Present
^{56}Sc	140.6(4), 187.9(5), 587.5(4), 728.0(6)	0.29(2)	37(8), 36(7), 100(18), 24(7)	Present
	47.7(3), 140.5(3), 187.8(3), 587.2(3), 727.1(3)	0.290(30)	70(19), 61(7), 61(8), 100(12), 32(5)	[51]

measurement. In the previous works using TOF- $B\rho$ method [39,49,50], it was reported that a correction depending on the atomic number is necessary to determine m/q values precisely. In the present analysis this correction was applied in the same manner as shown in Ref. [39]. The systematic errors of the Z -dependence correction for Sc, Ti, and V isotopes were evaluated to be 5.7, 9.1, and 13.3 keV/e, respectively.

Additionally we estimated the mass shifts contributed from isomers in the beam. Details of the isomer measurement were reported in Ref. [44]. The particles were stopped in the S2 plastic stopper after the mass measurement and the two HPGe detectors installed close to the stopper detected the isomeric γ rays (see Fig. 1). This system confirmed that the isomers in $^{56,58}\text{Sc}$ and $^{59,61}\text{Ti}$ were contained in the beams, where the isomeric γ spectra in ^{58}Sc and ^{61}Ti were previously reported [44]. The typical detection efficiency of the system was 10% (2%) for 100-keV (1-MeV) γ rays. The isomeric γ energies identified in the present experiment are summarized in Table I together with previously reported information [33,51]. The present values of γ -ray energies (E_γ), half lives ($T_{1/2}$), and relative intensities (I_γ) are consistent with the reported data, where I_γ includes the conversion electrons estimated by the BrIcc evaluation [52]. An isomer reported in ^{64}V [53] was not observed in the present experiment and hence the mass shift by this isomer was negligible. The contaminant fluxes of isomers (ϵ_{F3}) and the contributions to the atomic masses (δE_{iso}) were evaluated based on the above isomeric data and the obtained γ yields, and summed up in Table II. The column of ϵ_{F3} shows contaminant fluxes at the focal plane F3 (see Fig. 1) estimated from the γ -ray yields. The δE_{iso} values are estimated from E_x , $T_{1/2}$, and ϵ_{F3} by using the equation

$$\delta E_{\text{iso}} = \epsilon_{\text{F3}} E_x \left(\frac{\gamma T_{1/2}}{t \ln 2} \right) \left(1 - \exp \left[- \frac{t \ln 2}{\gamma T_{1/2}} \right] \right), \quad (2)$$

where t and γ are TOF and the Lorentz factor of the isomers, respectively. Because the isomeric state in ^{58}Sc could not be fully determined due to insufficient statistics, we evaluated δE_{iso} in all combinations. The mass shifts by the sub- μ s isomers in ^{56}Sc and $^{59,61}\text{Ti}$ were obtained from

the present isomeric γ -ray data, where the cascade effect in ^{61}Ti is considered. In ^{56}Sc , a high-spin isomeric state was reported [51], and the δE_{iso} estimation for this state is also shown in Table II. The E_x and ϵ_{F3} values of the state are estimated based on the experimental results of Ref. [51]. The ϵ_{F3} value can be estimated to be $\sim 50\%$, because their RI beams were produced by the fragmentation reactions under similar conditions. Also, it is assumed that the E_x value of this isomeric state is as high as that of the other isomer because of their spin assignments. If these energies would be very different, the γ transitions would, certainly, have been observed experimentally.

The present experiment successfully provides the atomic masses of $^{58-60}\text{Sc}$, $^{60-62}\text{Ti}$, and $^{62-64}\text{V}$ for the first time. The atomic mass excesses of the isotopes determined in the present experiment are summarized in Table III. The total error of a mass excess is obtained by a quadric sum of the statistical error, the two systematic errors and an estimated error in the mass shift by isomeric states. In the third column, the values cited in the AME2016 database [54] are shown, where those with a hash sign (#) are estimated values. The present mass excesses are fully consistent with the AME2016 database within 1σ errors. The recent results reported in Ref. [55] are shown in the fourth column, and are consistent with the present results.

To qualify the systematic trends of the mass surface in the interested nuclear region, Fig. 3 shows the two-neutron separation energies (S_{2n}) in the range of isotopes of $^{20}\text{Ca} - ^{26}\text{Fe}$. The S_{2n} value is defined as $S_{2n}(Z, N) = \Delta_m(Z, N - 2) - \Delta_m(Z, N) + 2\Delta_n$, where

 TABLE II. The estimated contributions of isomeric states to the atomic masses (δE_{iso}). The table includes the excitation energies (E_x), half lives ($T_{1/2}$), and fluxes of the isomeric states (ϵ_{F3}) deduced in the present experiment.

Nucleus	E_x (keV)	$T_{1/2}$ (μ s)	ϵ_{F3} (%)	δE_{iso} (keV)
^{61}Ti	701.3(7)	0.354(69)	28(11)	144(60)
	125.2(6)	0.200(28)	0(24)	
^{59}Ti	108.9(4)	0.618(12)	86(4)	73(3)
^{58}Sc	69(22)
^{56}Sc	775.0(1)	0.29(2)	3(1)	19(3)
	~ 775	$7.5(6) \times 10^4$	~ 50	0(390)

TABLE III. The atomic mass excesses determined in the present experiment and those cited in the AME2016 [54] and Ref. [55] are shown. The hash sign (#) indicates the estimated values in AME2016.

Nucleus	Present (keV)	AME2016 [54] (keV)	Ref. [55] (keV)
^{64}V	-16 690(510)	-16 320(400)#	...
^{63}V	-21 740(340)	-21 890(400)#	...
^{62}V	-25 130(340)	-25 480(300)#	...
^{61}V	-29 700(430)	-30 510(890)	-30 380(280)
^{62}Ti	-13 300(450)	-12 500(400)#	...
^{61}Ti	-16 180(280)	-16 350(400)#	...
^{60}Ti	-22 100(240)	-22 330(300)#	...
^{59}Ti	-25 200(240)	-25 510(200)#	-25 220(270)
^{58}Ti	-30 950(270)	-31 110(200)#	-30 890(250)
^{60}Sc	-3550(1040)	-4050(500)#	...
^{59}Sc	-10 830(250)	-10300(400)#	...
^{58}Sc	-15 480(190)	-14 880(400)#	...
^{57}Sc	-21 380(180)	-21 000(1300)	-20 180(890)
^{56}Sc	-25 310(430)	-24 850(590)	-25 380(260) ($^{+0}_{-540}$)
^{55}Sc	-30 610(190)	-30 160(450)	-31 090(220)

$\Delta_m(Z, N)$ and Δ_n are the mass excess of the isotope with Z protons and N neutrons and that of a neutron, respectively. The plots in this figure are calculated from the present masses, AME2016 database and the masses reported after AME2016 [32,39,55–57]. The solid (open) circles show the values listed in Table III (reported). Isotopic chains are connected by solid lines.

It is well known that the decreasing S_{2n} values of an isotope as a function of the neutron number is primarily linked to the asymmetry term in the liquid-drop model and to the configuration mixing promoted by the two-body interactions in the nuclear shell model. Both descriptions lead to an approximately linear drop of S_{2n} chains [58], and such a trend appears in chains of proton-magic isotopes such as the Ca and Ni isotopes. The deviation from linearity in a S_{2n} chain indicates the change of nuclear properties of the isotopes: A sudden drop of a S_{2n} value indicates a shell closure. An increasing trend of a S_{2n} chain indicates the emergence of the JT effect, where the correlation or deformation lower the ground-state energy of the isotope.

In Fig. 3, the S_{2n} trends in V-Fe isotopes are similar, decreasing gradually as the neutron number increases up to 40. Also, for $N = 34$ –37, the S_{2n} slopes of Ti and Sc isotopes are similar to heavier isotopes. The S_{2n} slope in Ti becomes almost constant horizontally for $N = 37$ –40, while the Sc chain continues a declining trend up to $N = 39$. The new value in ^{64}V shows that the V isotope has an open-shell nature at $N = 40$ as observed in Mn and Fe isotopes.

Figure 3 also shows a theoretical S_{2n} systematics obtained from a current global mass model. The dashed lines show the predictions of the macroscopic-microscopic

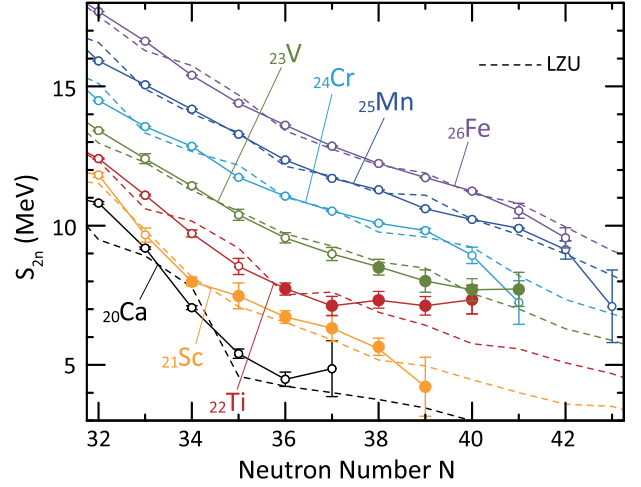


FIG. 3. The two-neutron separation energies (S_{2n}) of Ca-Fe isotopes around $N = 40$ as a function of the neutron number. The solid lines connect isotopes. The dashed lines show a theoretical prediction [59] as calculated by the LZU model.

Weizsäcker-Skyrme-type (WS-type) formula with treatments of two radial basis functions (RBF) corrections (LZU) [59], which is reported to reproduce the atomic masses listed in AME2016 with an accuracy of 149 keV in rms. The lines of the prediction are corresponding to the experimental data with the same colors. This model largely reproduces the S_{2n} trends including the present data. However, it is obvious that the model underestimates the S_{2n} values in $^{61,62}\text{Ti}$ isotopes.

Also in the following modern global mass models that reproduce the trends of the experimental S_{2n} values, a similar underestimation of S_{2n} is found around ^{62}Ti : WS4^{RBF} [60] and UNEDF1 [61]. WS4^{RBF} is a modified WS-type mass model having excellent mass reproductivity for experimental values, which is comparable to LZU (170 keV in rms for the AME2012 data). The WS4^{RBF} mass predictions in this region are almost identical to the LZU predictions. UNEDF1 is the recent universal nuclear energy density functional, which is updated from the UNEDF0 [62] by adding the experimental excitation energies of fission isomers in the actinides to the list of fit observables. UNEDF1 reproduces more quantitatively the S_{2n} trends around the present results. Although its reproductivity is worse than the above WS-type models (~ 1 MeV in rms for S_{2n} [63]), the calculated trends sufficiently match the experimental values except in the vicinity of ^{62}Ti . The S_{2n} systematics by all of those mass models correspond to the features of LZU. In Fig. 3, only the results of the LZU calculations are shown to avoid clutter.

The theoretical S_{2n} evaluations by the microscopic calculations with the valence-space formulation of the in-medium similarity renormalization group (VS-IMSRG) [64] were published recently. It was reported that the theoretical S_{2n} values are systematically smaller than the

experimental ones in Ca and Cr isotopes for $N > 34$ [32,39,55]. Also in comparison to the present results, the same trends were found in Ti and V isotope chains.

The experimental results reveal the emergence of a large JT effect in the vicinity of ^{62}Ti in comparison with the above-discussed theoretical predictions, and confirm that ^{62}Ti becomes very stable. Because the behavior of the mass surface resembles the one in the $N = 20$ island of inversion, it is natural to consider that the configuration mixing among neutron *fp* orbitals is advanced in the region, driving the onset of the island of inversion along $N = 40$. The expansion of configuration mixing in neutron orbitals was experimentally confirmed by the increasing of the quadrupole deformation in Fe and Cr isotopes at $N = 40$. The present experiment confirms the largest JT stabilization in the vicinity of ^{62}Ti , although the nuclear quadrupole deformation from Cr to Ti decreases [34]. This divergence is a unique feature at $N = 40$ and has not been observed in the neutron-rich deformation regions at $N = 8, 20$, and 28. It was theoretically discussed that an emergence of the nuclear JT effect is dominated by the ratio of residual interactions over an energy scale of the level degeneracy [4]. In this situation, the quadrupole-quadrupole interaction in nuclei is remarkable among the residual interactions. Therefore, the present results imply that the degeneracy of neutron single-particle states strongly promotes JT stabilization in ^{62}Ti , and that ^{62}Ti consequently obtains large nuclear stability in spite of relatively small deformation.

The experimental trend of S_{2n} in Sc isotopes suggests that the JT effect decreases towards ^{60}Ca . Almost all of the theoretical mass models cited above and the shell-model calculations [23] predict to be the open-shell nature in ^{60}Ca . However, the mass of ^{61}Sc and the improvement in ^{60}Sc are critical for quantitative discussions.

In conclusion, the atomic masses of the neutron-rich isotopes $^{58-60}\text{Sc}$, $^{60-62}\text{Ti}$, and $^{62-64}\text{V}$ were measured using the TOF- $B\rho$ method and determined for the first time. The relative precision of the atomic mass of ^{62}Ti was achieved to be 7.8×10^{-6} . The S_{2n} systematics extended through the present measurements exhibit that the JT effect is observed in the masses of $^{61,62}\text{Ti}$, and that the nuclei in the vicinity of ^{62}Ti have stabilities larger than predictions by current theoretical mass models. The recent experimental and theoretical studies [65,66] of neutron-rich Fe and Cr nuclei suggest that the deformation in the isotopes extends beyond $N = 40$ and reaches $N = 50$. Also, the existence of ^{60}Ca is experimentally confirmed and the existence of ^{70}Ca is theoretically expected [67]. To pin down these attractive expectations, it is a critical to know how far a large JT stability extends towards more neutron-rich isotopes as observed in ^{62}Ti . The extent of this effect may dominate the neutron drip line of not only neutron-rich Ti but also Ca isotopes.

We thank the RIKEN Nishina Center and the Center for Nuclear Study, the University of Tokyo accelerator staff for the excellent beam delivery. This work is financially supported in part by JSPS KAKENHI Grant No. JP22740150. M. K. is grateful to the JSPS for a Research Fellowship for young scientists under Program No. JP14J03376. G. P. A. B. acknowledges support by the National Science Foundation through Grant No. PHY-1068192 and The Joint Institute for Nuclear Astrophysics - Center for the Evolution of the Elements through Grants No. PHY-0822648 and No. PHY-1430152.

*mitimasa@cns.s.u-tokyo.ac.jp

†Present address: Korea Basic Science Institute, 169-148, Gwahak-ro, Yuseong-gu, Daejeon 34133, Korea.

‡Present Address: Research Center for Nuclear Physics, Osaka University, 10-1 Mihogaoka, Ibaraki, Osaka 567-0047, Japan.

§Present address: Department of Physics, Osaka University, 1-1 Machikaneyama-cho, Toyonaka, Osaka 560-0043, Japan.

||RIKEN Nishina Center for Accelerator-Based Science, 2-1 Hirosawa, Wako, Saitama 351-0198, Japan.

¶Institut für Kernphysik, Technische Universität Darmstadt, D-64289 Darmstadt, Germany.

**Rare Isotope Science Project, Institute for Basic Science 70, Yuseong-daero 1689-gil, Yuseong-gu, Daejeon, Korea.

- [1] M. G. Mayer, *Phys. Rev.* **75**, 1969 (1949).
- [2] O. Haxel, J. H. D. Jensen, and H. E. Suess, *Phys. Rev.* **75**, 1766 (1949).
- [3] H. A. Jahn and E. Teller, *Proc. R. Soc. A* **161**, 220 (1937).
- [4] P.-G. Reinhard and E. W. Otten, *Nucl. Phys.* **A420**, 173 (1984).
- [5] J. H. Van Vleck, *J. Chem. Phys.* **7**, 72 (1939).
- [6] O. Sorlin and M.-G. Porquet, *Prog. Part. Nucl. Phys.* **61**, 602 (2008).
- [7] A. Navin *et al.*, *Phys. Rev. Lett.* **85**, 266 (2000).
- [8] H. Iwasaki *et al.*, *Phys. Lett. B* **481**, 7 (2000).
- [9] H. Iwasaki *et al.*, *Phys. Lett. B* **491**, 8 (2000).
- [10] C. Thibault, R. Klapisch, C. Rigaud, A. M. Poskanzer, R. Prieels, L. Lessard, and W. Reisdorf, *Phys. Rev. C* **12**, 644 (1975).
- [11] D. Guillemaud-Mueller, C. Detraz, F. Naulin, M. de Saint-Simon, C. Thibault, F. Touchard, and M. Epherre, *Nucl. Phys.* **A426**, 37 (1984).
- [12] T. Motobayashi, Y. Ikeda, K. Ieki, M. Inoue, N. Iwasa, T. Kikuchi, M. Kurokawa, S. Moriya, S. Ogawa, H. Murakami, S. Shimoura, Y. Yanagisawa, T. Nakamura, Y. Watanabe, M. Ishiharab, T. Teranishi, H. Okuno, and R. F. Casten, *Phys. Lett. B* **346**, 9 (1995).
- [13] T. Glasmacher, B. A. Brown, M. J. Chromik, P. D. Cottle, M. Fauerbach, R. W. Ibbotson, K. W. Kemper, D. J. Morrissey, H. Scheit, D. W. Sklenicka, and M. Steiner, *Phys. Lett. B* **395**, 163 (1997).
- [14] F. Sarazin *et al.*, *Phys. Rev. Lett.* **84**, 5062 (2000).
- [15] B. Bastin *et al.*, *Phys. Rev. Lett.* **99**, 022503 (2007).
- [16] S. Takeuchi *et al.*, *Phys. Rev. Lett.* **109**, 182501 (2012).
- [17] B. A. Brown, *Prog. Part. Nucl. Phys.* **47**, 517 (2001).

- [18] E. K. Warburton, J. A. Becker, and B. A. Brown, *Phys. Rev. C* **41**, 1147 (1990).
- [19] T. Otsuka, R. Fujimoto, Y. Utsuno, B. A. Brown, M. Honma, and T. Mizusaki, *Phys. Rev. Lett.* **87**, 082502 (2001).
- [20] T. Otsuka, T. Suzuki, R. Fujimoto, H. Grawe, and Y. Akaishi, *Phys. Rev. Lett.* **95**, 232502 (2005).
- [21] N. A. Smirnova, B. Bally, K. Heyde, F. Nowacki, and K. Sieja, *Phys. Lett. B* **686**, 109 (2010).
- [22] M. Honma, T. Otsuka, B. A. Brown, and T. Mizusaki, *Eur. Phys. J. A* **25**, 499 (2005).
- [23] S. M. Lenzi, F. Nowacki, A. Poves, and K. Sieja, *Phys. Rev. C* **82**, 054301 (2010).
- [24] M. Hannawald, T. Kautzsch, A. Wöhr, W. B. Walters, K.-L. Kratz, V. N. Fedoseyev, V. I. Mishin, W. Böhmer, B. Pfeiffer, V. Sebastian, Y. Jading, U. Köster, J. Lettry, H. L. Ravn (The ISOLDE Collaboration), *Phys. Rev. Lett.* **82**, 1931 (1999).
- [25] O. Sorlin *et al.*, *Eur. Phys. J. A* **16**, 55 (2003).
- [26] P. Adrich, A. M. Amthor, D. Bazin, M. D. Bowen, B. A. Brown, C. M. Campbell, J. M. Cook, A. Gade, D. Galaviz, T. Glasmacher, S. McDaniel, D. Miller, A. Obertelli, Y. Shimbara, K. P. Siwek, J. A. Tostevin, and D. Weisshaar, *Phys. Rev. C* **77**, 054306 (2008).
- [27] N. Aoi *et al.*, *Phys. Rev. Lett.* **102**, 012502 (2009).
- [28] J. Ljungvall *et al.*, *Phys. Rev. C* **81**, 061301(R) (2010).
- [29] H. L. Crawford *et al.*, *Phys. Rev. Lett.* **110**, 242701 (2013).
- [30] S. Naimi, G. Audi, D. Beck, K. Blaum, Ch. Böhm, Ch. Borgmann, M. Breitenfeldt, S. George, F. Herfurth, A. Herlert, A. Kellerbauer, M. Kowalska, D. Lunney, E. Minaya Ramirez, D. Neidherr, M. Rosenbusch, L. Schweikhard, R. N. Wolf, and K. Zuber, *Phys. Rev. C* **86**, 014325 (2012).
- [31] Z. Meisel *et al.*, *Phys. Rev. C* **93**, 035805 (2016).
- [32] M. Mougeot *et al.*, *Phys. Rev. Lett.* **120**, 232501 (2018).
- [33] K. Wimmer *et al.*, *Phys. Lett. B* **792**, 16 (2019).
- [34] M. L. Cortés *et al.*, *Phys. Lett. B* **800**, 135071 (2020).
- [35] A. Gillibert, L. Bianchi, A. Cunsolo, B. Fernandez, A. Foti, J. Gastebois, C. Gregoire, W. Mittig, A. Peghaire, Y. Schutz, and C. Stephan, *Phys. Lett. B* **176**, 317 (1986).
- [36] D. J. Vieira, J. M. Wouters, K. Vaziri, R. H. Kraus, H. Wollnik, G. W. Butler, F. K. Wohn, and A. H. Wapstra, *Phys. Rev. Lett.* **57**, 3253 (1986).
- [37] T. Kubo, *Nucl. Instrum. Methods Phys. Res., Sect. B* **204**, 97 (2003).
- [38] T. Uesaka, S. Shimoura, and H. Sakai, *Prog. Theor. Exp. Phys.* **2012**, 03C007 (2012).
- [39] S. Michimasa *et al.*, *Phys. Rev. Lett.* **121**, 022506 (2018).
- [40] S. Michimasa *et al.*, *Nucl. Instrum. Methods Phys. Res., Sect. B* **317**, 305 (2013).
- [41] S. Michimasa, M. Takaki, M. Dozono, S. Go, H. Baba, E. Ideguchi, K. Kisamori, H. Matsubara, H. Miya, S. Ota, H. Sakai, S. Shimoura, A. Stolz, T. L. Tang, H. Tokieda, T. Uesaka, and R. G. T. Zegers, *Nucl. Instrum. Methods Phys. Res., Sect. B* **317**, 710 (2013).
- [42] H. Miya, S. Ota, T. Fujii, S. Kawase, Y. Kubota, C. S. Lee, H. Matsubara, K. Miki, A. Saito, S. Michimasa, T. Uesaka, H. Sakai, and S. Shimoura, *Nucl. Instrum. Methods Phys. Res., Sect. B* **317**, 701 (2013).
- [43] H. Kumagai, A. Ozawa, N. Fukuda, K. Sümmerer, and I. Tanihata, *Nucl. Instrum. Methods Phys. Res., Sect. A* **470**, 562 (2001).
- [44] S. Michimasa *et al.*, *Proc. Sci., INPC2016* (2017) 106.
- [45] K. Hosomi *et al.*, *Prog. Theor. Exp. Phys.* **2015**, 081D01 (2015).
- [46] M. Wang, G. Audi, A. H. Wapstra, F. G. Kondev, M. MacCormick, X. Xu, and B. Pfeiffer, *Chin. Phys. C* **36**, 1603 (2012).
- [47] F. Wienholtz *et al.*, *Nature (London)* **498**, 346 (2013).
- [48] M. Rosenbusch *et al.*, *Phys. Rev. Lett.* **114**, 202501 (2015).
- [49] Z. Meisel *et al.*, *Phys. Rev. Lett.* **114**, 022501 (2015).
- [50] M. Matoš, A. Estradé, H. Schatz, D. Bazin, M. Famiano, A. Gade, S. George, W. G. Lynch, Z. Meisel, M. Portillo, A. Rogers, D. Shapira, A. Stolz, M. Wallace, and J. Yurkon, *Nucl. Instrum. Methods Phys. Res., Sect. A* **696**, 171 (2012).
- [51] H. L. Crawford, R. V. F. Janssens, P. F. Mantica, J. S. Berryman, R. Broda, M. P. Carpenter, N. Cieplicka, B. Fornal, G. F. Grinyer, N. Hoteling, B. P. Kay, T. Lauritsen, T. Minamisono, I. Stefanescu, J. B. Stoker, W. B. Walters, and S. Zhu, *Phys. Rev. C*, **82**, 014311 (2010).
- [52] T. Kibédi, T. W. Burrows, M. B. Trzhaskovskaya, P. M. Davidson, and C. W. Nestor Jr., *Nucl. Instrum. Methods Phys. Res., Sect. A* **589**, 202 (2008).
- [53] S. Suchyta, S. N. Liddick, C. J. Chiara, W. B. Walters, M. P. Carpenter, H. L. Crawford, G. F. Grinyer, G. Gürdal, A. Klose, E. A. McCutchan, J. Pereira, and S. Zhu, *Phys. Rev. C* **89**, 067303 (2014).
- [54] M. Wang, G. Audi, F. G. Kondev, W. J. Huang, S. Naimi, and X. Xu, *Chin. Phys. C* **41**, 030003 (2017).
- [55] Z. Meisel *et al.*, *Phys. Rev. C* **101**, 052801(R) (2020).
- [56] E. Leistenschneider *et al.*, *Phys. Rev. Lett.* **120**, 062503 (2018).
- [57] X. Xu *et al.*, *Phys. Rev. C* **99**, 064303 (2019).
- [58] R. Fossion, C. De Coster, J. E. Garía-Ramos, T. Werner, and K. Heyde, *Nucl. Phys. A* **697**, 703 (2002).
- [59] N.-N. Ma, H.-F. Zhang, X.-J. Bao, and H.-F. Zhang, *Chin. Phys. C* **43**, 044105 (2019).
- [60] N. Wang, M. Liu, X. Z. Wu, and J. Meng, *Phys. Lett. B* **734**, 215 (2014).
- [61] M. Kortelainen, T. Lesinski, J. More, W. Nazarewicz, J. Sarich, N. Schunck, M. V. Stoitsov, and S. Wild, *Phys. Rev. C* **85**, 024304 (2012).
- [62] M. Kortelainen, T. Lesinski, J. Moré, W. Nazarewicz, J. Sarich, N. Schunck, M. V. Stoitsov, and S. Wild, *Phys. Rev. C* **82**, 024313 (2010).
- [63] M. Kortelainen, J. McDonnell, W. Nazarewicz, E. Olsen, P.-G. Reinhard, J. Sarich, N. Schunck, S. M. Wild, D. Davesne, J. Erler, and A. Pastore, *Phys. Rev. C* **89**, 054314 (2014).
- [64] J. D. Holt, S. R. Stroberg, A. Schwenk, and J. Simonis, *arXiv:1905.10475v1*.
- [65] C. Santamaria *et al.*, *Phys. Rev. Lett.* **115**, 192501 (2015).
- [66] F. Nowacki, A. Poves, E. Caurier, and B. Bounthong, *Phys. Rev. Lett.* **117**, 272501 (2016).
- [67] O. B. Tarasov *et al.*, *Phys. Rev. Lett.* **121**, 022501 (2018).